Spatial and energetic-entropic decomposition of surface tension in lipid bilayers from molecular dynamics simulations

Erik Lindahl and Olle Edholm[a)]
Theoretical Physics, Royal Institute of Technology, SE-100 44 Stockholm, Sweden

(Received 10 February 2000; accepted 1 June 2000)

The spatial and groupwise distribution of surface tension in a fully hydrated 256 lipid dipalmitoylphosphatidylcholine (DPPC) bilayer is determined from a 5 ns molecular dynamics simulation by resolving the normal and lateral pressures in space through the introduction of a local virial. The resulting surface tension is separated into contributions from different types of interactions and pairwise terms between lipid headgroups, chains and water. By additionally performing a series of five simulations at constant areas ranging from 0.605 to 0.665 nm^2 (each of 6 ns length), it is possible to independently resolve the energetic contributions to surface tension from the area dependence of the interaction energies. This also enables us to calculate the remaining entropic part of the tension and the thermal expansivity. Together with the total lateral pressures this yields a full decomposition of surface tension into energetic and entropic contributions from electrostatics, Lennard-Jones and bonded interactions between lipid chains, headgroups and water molecules. The resulting total surface tension in the bilayer is found to be a sum of very large terms of opposing signs, explaining the sensitivity of simulation surface tension to details in force fields. Headgroup and headgroup–water interactions are identified as attractive on average while the chain region wants to expand the bilayer. Both effects are dominated by entropic contributions but there are also substantial energetic terms in the hydrophobic core. The net lateral pressure is small and relatively smooth compared to the individual components, in agreement with experimental observations of DPPC lipids forming stable bilayers. © *2000 American Institute of Physics.* [S0021-9606(00)50333-X]

I. INTRODUCTION

Phospholipid bilayers constitute one of the key building blocks in cellular systems where they are responsible for virtually all wall structures. They have fascinating properties which nonetheless are slightly contradictory; on one hand they exhibit an extreme flexibility and two-dimensional liquid behavior which makes it possible to insert proteins like ion channels in the structure, and on the other they are remarkably stable and efficient as interfacial barriers.[1–3]

These characteristics come from the fact that the bilayer itself is an assembly of separate molecules, with large relative motions of individual lipids and thermally excited collective undulatory fluctuations.[4,5] The stability is usually attributed to a balance between the hydrophobic effect on the exposure of lipid chains to water—a process striving to decrease the area of the membrane, and intermolecular interactions inside the membrane which favor a larger area (see, e.g., the review by Marsh[6]). If the contracting force in the headgroups was considerably weaker or stronger than the opposing one in the membrane interior the lipids would not form planar bilayers but rather micelles or hexagonal phases. This balance results in a free energy which varies weakly with surface area, reflected in that it is one to two orders of magnitude easier to change the surface area of a bilayer at constant volume with an accompanying change in thickness than to change the bilayer's volume.

Since the locations of the contracting and expanding forces are separated by less than 1–2 nm in a bilayer it is not easy to study them separately through experiments, which makes our knowledge about them limited. Molecular dynamics simulation of bilayers is an attractive alternative by which it is possible to examine interactions like these at atomic level. Although this is still limited to relatively small systems and short time scales, large progress has been made in the last few years, and membrane simulations are now reasonably accurate in describing many properties like, e.g., volume per lipid and the structure in the crystalline and gel phases.[7–10] Other experimental results have been more problematic to reproduce, though; it seems as if very small differences in simulation force fields can produce unexpectedly large variations in some observed properties of the system. The most notable example is the equilibrium area per lipid in the liquid crystalline phase or, in the case of constant area, the conjugate thermodynamic variable surface tension.[10–12] Such discrepancies could probably be tolerated if it was not for the case that they also affect many other quantities strongly coupled to the area like the order parameters and fraction *gauche* bonds in the lipid chains, and possibly also the chain dynamics. These observations have led to some argumentation[13,14] whether the periodic boundary conditions in a finite-size simulated bilayer system makes it necessary to apply a surface tension to mimic an unstressed state in a

a)Author to whom correspondence should be addressed. Electronic mail: oed@theophys.kth.se; phone: +46-8-7907164; Fax: +46-8-104879.

subpatch of a macroscopic sized flaccid vesicle. (In the macroscopic case it is clear that a bilayer free to adjust its area and not subject to osmotic stress has zero surface tension.[14])

Although there are many interesting aspects of this discussion, the single most important conclusion is that the lateral tension in a liquid crystalline bilayer is very sensitive to the details in simulation setup. In our opinion this is however not very surprising considering the assumed balance between contraction and expansion in bilayers mentioned above. Since the resulting surface tension will come out as a small difference between these terms, minor changes in interaction parameters could easily shift the relative weight between contracting and expanding forces, yielding slightly different equilibrium states. To examine this it is necessary to resolve the separate terms in the total surface tension. Another motivation to study them is that the magnitude and origin of the contributions, including their spatial location in the bilayer, also determine the elastic properties of the assembly, and whether the lipids prefer to form planar membranes or micelles. Unfortunately this is not trivial to determine even in computer simulations since normally only the total surface tension in the system can be resolved.

In the present work we introduce a method to decompose the net surface tension in molecular dynamics simulations of membrane systems. By replacing the ordinary virial used for calculating the pressure with a corresponding expression resolved locally in space it is possible to extract curves with the local normal and lateral pressures, and thus calculate surface tension as a function of the normal coordinate in the bilayer. This total surface tension is a combination of energetic and entropic terms, but the division is not accessible from the virial. It is however possible to circumvent this limitation and determine the energetic parts of the surface tension independently by performing several simulations at different areas for the same system and calculate the energetic tension contributions from the area dependence of the interaction energies. Since we already know the full tension, this makes it trivial to solve also for the remaining entropic part.

This is applied to a fully hydrated 256 lipid dipalmitoylphosphatidylcholine (DPPC) bilayer which we simulate for 5 ns in the liquid crystalline phase with a local virial at an area of 0.635 nm^2/lipid. We also perform five further simulations of the same system at constant areas ranging from 0.605 to 0.665 nm^2 per lipid in order to determine the area dependence of interaction energies. The energies and local virial tensors are calculated separately for electrostatics, Lennard-Jones interactions, dihedral rotations around chain bonds and other bonded forces. It is further refined into contributions from all pairwise combinations of lipid chains, headgroups and water molecules.

These simulations provide us with a total division of the surface tension in a real membrane system into energetic and entropic terms from all different types of interactions between pairs of the above mentioned groups, and they make it possible to estimate how the measured average surface tension is distributed inside the bilayer and its interfacial regions. It is also possible to calculate the thermal expansivity coefficient for the bilayer from the entropic part of the surface tensions. The resulting observations from the simulations are compared with experiments and simplified theoretical models of membranes and we consider the implications for the stability of the bilayer. We also discuss the relation to the sensitive dependence on force field parameters and to which extent the findings are significant or applicable to other bilayers or lipid assemblies in general.

II. THEORY

A. Local pressure

The tension along a surface is defined as the derivative of free energy as a function of area, $\gamma=(\partial F/\partial A)$. This can be defined either per surface or for the whole bilayer; in this work we consistently use the latter alternative. In a simulation it is usually calculated from the difference between the normal $[p_N=p_{zz}]$ and lateral $[p_L=(p_{xx}+p_{yy})/2]$ components of the pressure tensor[15]

$$\gamma=\int [p_N(z)-p_L(z)]dz. \tag{2.1}$$

Strictly, this expression is valid only in equilibrium when the pressure tensor is diagonal on average. For a liquid or liquid crystalline system this is essentially always fulfilled in molecular dynamics simulations, but care should be taken before applying the formula to solid systems. The scalar average pressure equals a third of the trace of the pressure tensor $\mathbf{p}$, which in turn is defined by

$$\mathbf{p}=2\langle\mathbf{E}\rangle-\boldsymbol{\Sigma}, \tag{2.2}$$

where the brackets denote ensemble averages. $\mathbf{E}$ is the kinetic energy density tensor and $\boldsymbol{\Sigma}$ the system's configurational stress tensor. The kinetic energy is obtained from the velocities of the particles

$$\mathbf{E}=\frac{1}{2}\sum_i m_i\mathbf{v}_i\otimes\mathbf{v}_i, \tag{2.3}$$

where the $\otimes$ sign denotes a tensor product. The configurational stress $\boldsymbol{\Sigma}$ is the (macroscopic) ensemble average of a corresponding microscopic entity describing the interaction force contributions to the pressure. In molecular dynamics simulations this ensemble average is calculated through the molecular virial $\boldsymbol{\Xi}$ as

$$\boldsymbol{\Sigma}=\frac{\boldsymbol{\Xi}}{V}=\frac{1}{V}\sum_{i<j}\mathbf{F}_{ij}\otimes\mathbf{r}_{ij}, \tag{2.4}$$

where $\mathbf{r}_{ij}$ and $\mathbf{F}_{ij}$ are the distance and force, respectively, between particles i and j. Since Eq. (2.4) is a pair-additive double sum over all particles it is well defined as a system average, but the expression will be ambiguous at scales below the range of forces. [Equation (2.4) will be modified when using lattice sums to calculate forces, in which case there will be a contribution to the virial from each wavevector in reciprocal space.[16] These individual terms will not be pair-additive over atoms in any simple way, but the system average is still defined and pair-additive as long as the sum in Eq. (2.4) over the infinite replications of the system is convergent.] This is reasonable, since pressure is an inher-

ently macroscopic feature. It is however possible to extend the definition to molecular scales by replacing Eq. (2.2) with a more general expression that can be evaluated unambiguously on smaller length scales while still providing the classical result for the entire system. It is important to realize that this is not necessarily a unique extension; we can in principle choose any definition as long as the correct pressure is still obtained in the macroscopic limit. Although the resulting total pressures agree their spatial distributions may differ, but the differences should be considerably smaller than the range of interactions for all reasonable alternatives.

Appendix A contains a deduction of one such possible extension of pressure definition. The kinetic energy tensor is straightforward to generalize to atomic scales since it is a single sum over pointlike energy contributions in space; when calculating local pressure the sum is just limited to the atoms present in the current region in space. The configurational stress tensor is slightly more complicated. The model introduced in the appendix leads to a *uniform* distribution of the virial from each interacting pair of particles along a curve in space connecting the two positions. Choosing a straight line for the curve is reasonable and relatively obvious, but nevertheless arbitrary. Other choices will yield slightly different distributions of local pressure, but considering the range and distance dependence of typical atomic interactions it should be possible to define the physical pressure uniquely down to a resolution of at least about 1 nm. Since it is not straightforward to derive a corresponding expression for lattice sums the local virial has to be calculated by direct space evaluation of Eq. (2.4).

For a membrane system it suffices to determine normal and lateral pressure components as a function of the normal coordinate. Dividing the simulation box into horizontal slices (of approximately 0.1 nm thickness) we obtain the local pressure tensor in a slice as

$$\mathbf{p}_{\text{local}}(z)=\sum_{i\in\text{slice}} m_i\mathbf{v}_i\otimes\mathbf{v}_i-\frac{1}{\Delta V}\sum_{i<j}\mathbf{F}_{ij}\otimes\mathbf{r}_{ij}f(z,z_i,z_j). \tag{2.5}$$

The first sum extends over all particles in the slice while the second is over all particle pairs in the system; ΔV is the volume of each slice with thickness Δz. The function f determines the amount of the virial to be located to the current slice; if both particles i and j are inside it we have $f=1$ and place the whole virial there. If both particles are outside the current slice on opposite sides (using periodic boundary conditions and considering the shortest distance between them) we set $f=\Delta z/|z_i-z_j|$, and when one of them is in the current slice it is changed to $f=\Delta z/2|z_i-z_j|$.

Theoretically, it should be possible to disregard the contribution from the average kinetic energy tensor, since it should be isotropic and the surface tension thus depend only on the configurational stress in a real system. This is however not necessarily the case in a simulation, where kinetic energy is often removed from bonds by keeping their lengths constant, or by losses in fast bond vibrations due to imperfect integration algorithms. The resulting discrepancy will not be noticeable in most systems, but due to the substantial ordering of the chain bonds along the normal direction in bilayers, such systems will exhibit a non-negligible anisotropy in kinetic energy. In the case of constant bond lengths the resulting tension will still be correct if the kinetic energy term is explicitly calculated though, since the constraint algorithm is just moving degrees of freedom from energy to interactions.

B. Surface tension decomposition

The free energy of the bilayer system can be separated into an energetic and an entropic part

$$F=U-TS. \tag{2.6}$$

Since the energy is additive this can be written as a sum of different types of interactions and a double sum over disjoint groups of atoms,

$$F=\sum_i\sum_{j,k}F_{i,jk}=\sum_i\sum_{j,k}(U_{i,jk}-TS_{i,jk}), \tag{2.7}$$

where $U_{i,jk}$ is the energy of interaction type i between groups j and k, and $S_{i,jk}$ the associated entropy. Similarly, the surface tension defined as the area derivative of the free energy at constant normal pressure and temperature may be split in parts,

$$\begin{aligned}\gamma=\sum_i\sum_{j,k}\gamma_{i,jk}&=\sum_i\sum_{j,k}\frac{\partial F_{i,jk}}{\partial A}\\&=\sum_i\sum_{j,k}\left(\frac{\partial U_{i,jk}}{\partial A}-T\frac{\partial S_{i,jk}}{\partial A}\right)\\&=\sum_i\sum_{j,k}(\gamma^U_{i,jk}+\gamma^S_{i,jk}),\end{aligned} \tag{2.8}$$

and it is thus appropriate to talk about groupwise energetic contributions $\gamma^U_{i,jk}$ to the surface tension and corresponding entropic terms $\gamma^S_{i,jk}$. The energetic surface tensions can be determined from the area dependence of interaction energies,

$$\gamma^U_{i,jk}=\frac{\partial U_{i,jk}}{\partial A}, \tag{2.9}$$

as the slope of a linear regression of energy versus area per lipid, which is obtained by simulating the system at several different areas. Since the total partial surface tensions $\gamma_{i,jk}$ are known from the local virial this trivially gives the entropic contributions as $\gamma^S_{i,jk}=\gamma_{i,jk}-\gamma^U_{i,jk}$. It is important to realize, though, that the decomposition of entropy is somewhat artifical since it per definition is a secondary effect of the interactions and cannot directly be attributed to individual forces. It is nevertheless valid in cases where the dynamics in the different groups or interactions are essentially independent of each other.

The entropic surface tension also provides a way to determine the thermal expansivity coefficient of the system. The total differential of the surface tension as a function of area and temperature can be written as

$$d\gamma=\frac{\partial\gamma}{\partial A}dA+\frac{\partial\gamma}{\partial T}dT. \tag{2.10}$$

The first derivative can be replaced with the area compressibility $K_A = A(\partial\gamma/\partial A)$, while we rewrite the second one as

$$\frac{\partial \gamma}{\partial T} = \frac{\partial^2 F}{\partial A \partial T} = \frac{\partial}{\partial A}\left(\frac{\partial F}{\partial T}\right) = -\frac{\partial S}{\partial A}. \tag{2.11}$$

From Eq. (2.8) we identify this as $(\partial S/\partial A) = -(1/T)\gamma^S$. Since the surface tension is constant at equilibrium we have

$$0 = d\gamma = \frac{K_A}{A}\, dA + \frac{1}{T}\gamma^S dT. \tag{2.12}$$

This finally makes it possible to solve for the bilayer thermal expansivity and calculate it from the total entropic contribution to surface tension,

$$\alpha = \frac{1}{A}\left(\frac{\partial A}{\partial T}\right)_{\gamma} = -\frac{\gamma^S}{TK_A}. \tag{2.13}$$

III. SIMULATIONS

The molecular dynamics force field employed builds on GROMOS (Refs. 17,18) bonded interaction parameters. Charges for the DPPC lipids in this force field were calculated by Chiu *et al.* using *ab initio* quantum chemistry.[19] United atoms and Ryckaert–Bellemans dihedrals[20] are used to describe the hydrocarbon chains.

Berger *et al.* observed that this, as well as many other force fields, produces slightly too high bilayer densities.[11] This lead them to reparameterize the chain nonbonded interactions starting from the OPLS parameters.[21] Since the OPLS carbon parameters are derived for smaller compounds they were adjusted slightly to reproduce density and heat of vaporization (the standard choice in OPLS) of liquid pentadecane.[11] This final choice of force field was shown to successfully reproduce the volume per lipid (the most accurately determined experimental quantity) within 1%, but also area per lipid and order parameters in the liquid crystalline phase.

To reduce the influence of the observed finite size effect in bilayer simulations[13,5] it is necessary to use a relatively large system. The starting structure was taken from the end frame of an earlier 5 ns simulation of a bilayer with 256 DPPC lipids, for which the finite size effect on area is less than 1%.[5] The (x,y) coordinates of this structure were scaled to produce 5 systems with areas per lipid of 0.605, 0.620, 0.635, 0.650, and 0.665 nm^2. The bilayers were hydrated with 23 SPC waters per lipid, bringing the systems to 30464 atoms each. Temperature was coupled to 323 K for lipids and water separately by using a Berendsen heat bath[22] with a time constant of 0.1 ps, and the normal pressure of the system adjusted to 1 atm by scaling the box z coordinate with a time constant of 1 ps. All simulations were carried out in parallel on 16 IBM SP2 processors at PDC, Stockholm, with the GROMACS (Ref. 23) molecular dynamics software. A time step of 2 fs was employed with all bond lengths kept constant using the LINCS (Ref. 24) algorithm and the analytical SETTLE (Ref. 25) for water. A cutoff at 1.0 nm was used for the Lennard-Jones interactions and 1.8 nm for electrostatics, the long-range Coulombic forces being updated every 10 steps. 1,4 electrostatic interactions were reduced a factor of 2 and Lennard-Jones interactions a factor of 8, according to the OPLS scheme. The systems were simulated for 6 ns, the first nanosecond of which was regarded as equilibration since the initial surface tension in the bilayer will mainly be a linear response to the applied change in area. Although both the box z-dimension and surface tension converge in a couple of 100 ps, other quantities like the electrostatic interactions between headgroups and water take substantially longer, up to a nanosecond. There are also slow undulatory and peristaltic oscillations in the bilayer[5] which makes it necessary with simulations of this length to obtain reliable data.

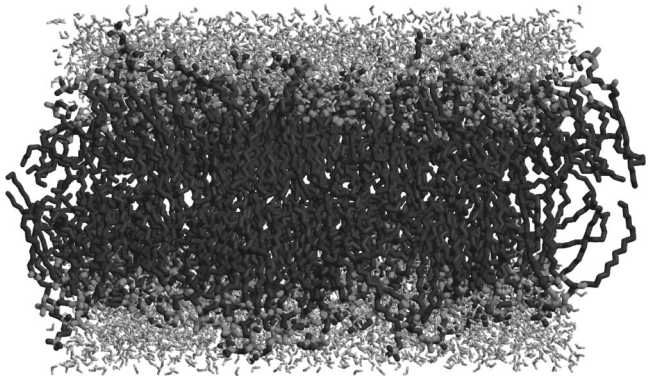

FIG. 1. A snapshot of the system at 6 ns. The lipids are drawn with thick rods, darker corresponding to carbon atoms and lighter to charged atoms in the headgroups. Water is represented as thin lines.

For the system with area 0.635 nm^2/lipid the z-dependent pressure tensor was calculated by implementing a local virial in the molecular dynamics software according to Appendix A and accumulating data from 60 slices in the z-direction every time step. This was decomposed into interaction types and pairwise contributions from lipid headgroups (charged atoms), chains (uncharged atoms), and water. Since the local virial computation makes the simulation several times slower the full precision trajectory of the previous simulation without local virial was used and runs restarted on 80 independent processors from the trajectory frames stored every 20 ps. Since LINCS does not directly yield pairwise forces the equivalent but slightly slower SHAKE (Ref. 26) algorithm was used in this simulation.

IV. RESULTS

A. Equilibrium properties

As the size of the system simulated grows, so do the fluctuations of extensive quantities. Most relative fluctuations will be smaller, but the root-mean-square (RMS) amplitude of mesoscopic dynamics in form of undulatory and peristaltic motions[27–29] will increase with system size. Figure 1 shows the end frame of the 0.635 nm^2/lipid system. There is a considerable roughening of the surface and intercalating chains in the hydrophobic moiety. The RMS spread in lipid z-coordinate defined from the position of the carbon atom connecting the chains to the headgroup is 0.28 nm. This shows a linear dependence on system side[5] and there will be a corresponding broadening of the density profiles compared

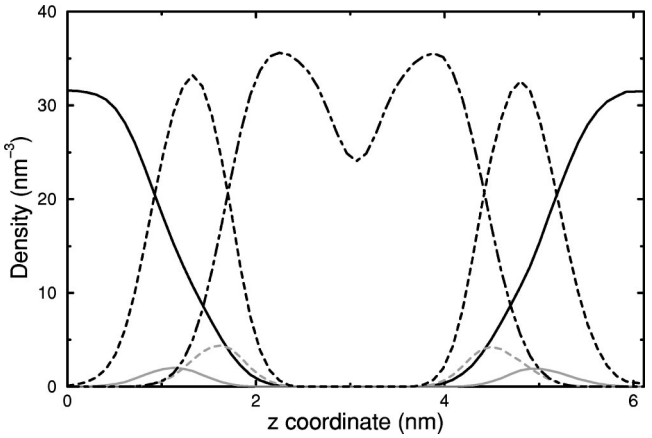

FIG. 2. Density distribution of water (solid black), headgroup atoms (dashed black), and lipid chain atoms (dotted–dashed black). The headgroup distribution is also shown as whole units of phosphocholine dipoles (solid gray), and carbonyl dipoles (dashed gray).

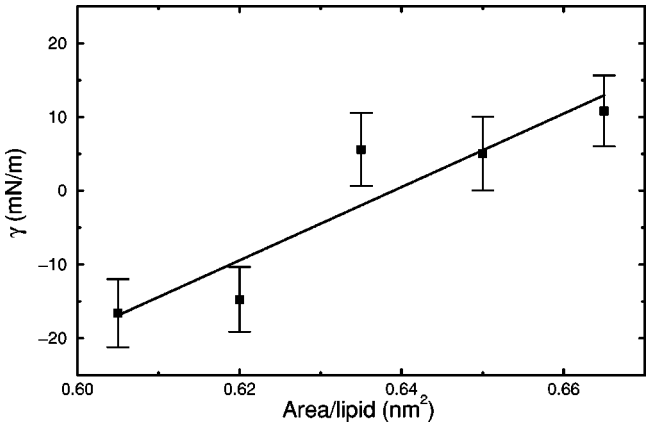

FIG. 4. Average bilayer surface tension vs equilibrium area/lipid. The error bars are calculated from fluctuations corrected for their autocorrelation times. The fitted area dependence yields $K_A \approx 300$ mN/m.

to simulations of smaller patches.[11] These density distributions are displayed in Fig. 2 for lipid chains, headgroups and water. Also included are positions of whole units of the large phosphocholine dipoles at the water interface and the two smaller carbonyl dipoles further inside the membrane. There is approximately one water molecule per chain as far in as the carbonyl dipoles and eight per lipid at the position of the phosphocholine dipole. The density of water attains its bulk value slightly before the box sides. Water molecules penetrate deep into the headgroups, but they do not enter the hydrophobic core; the solvent density vanishes with the carbonyl groups. The statistical accuracies in monitored quantities were determined from the fluctuations corrected for their autocorrelation times which range from 5 ps for bond energies to over a nanosecond for the surface tension. Typical estimated standard errors and total drifts in energies were in the order of 1 kJ/mol lipid, which for the total energy corresponds to less than 0.05%.

The time dependence of the total bilayer surface tension in the five systems during the simulations is displayed as 0.5 ns running averages in Fig. 3. Even after the first nanosecond of relaxation there are large fluctuations with autocorrelation times in the nanosecond range, explaining the large statistical errors. The average surface tension in each system is plotted vs area per lipid in Fig. 4. Using the formula

$$K_A = A \frac{\partial \gamma}{\partial A}, \tag{4.1}$$

a bilayer area compressibility of $K_A = 300 \pm 50$ mN/m is obtained from the fitted curve. This K_A is a direct (true intrinsic) area compressibility, in contrast to the apparent experimental value $\overline{K}$ which also contains contributions from the long wavelength membrane undulations which are largely suppressed in the simulation. Apparent bilayer compressibilities for different lecithin lipids have been measured[30] in the range 135–190 mN/m, but when corrected for the bending undulations [Eq. (4) in Evans *et al.*[30]] the direct bilayer area compressibilities K_A are in the range 230–250 mN/m for both saturated and unsaturated lipids,[31] which agrees reasonably well with our simulated value. This corresponds to 2×10^{-3} atm^{-1}, which is a factor 40 larger than the bilayer's volume compressibility.[11] The equilibrium area of the system at zero surface tension would be in the 0.63–0.64 nm^2 range. This area compressibility can alternatively be extracted from the fluctuations in area at constant surface tension; our earlier simulations yielded a value similar to the present one using this approach.[5] However, the two methods are not trivially equivalent and require very long runs like the present ones to yield accurate values since we in practice are measuring a second derivative of the free energy. This has recently been demonstrated by Feller and Pastor[12] who calculated K_A with several methods producing values ranging from 220 to about 1600 mN/m for a bilayer.

It is instructive to calculate the free energy variation around the equilibrium area A_0. Integrating Eq. (4.1) we obtain

$$\gamma = K_A \ln A/A_0 \approx K_A \frac{A - A_0}{A_0}. \tag{4.2}$$

If this is integrated once more the free energy becomes

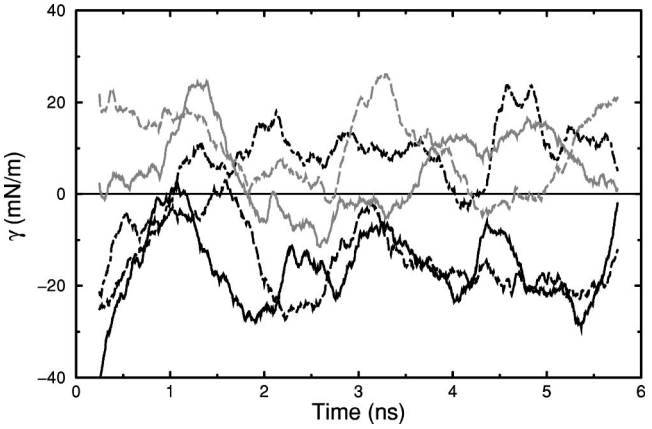

FIG. 3. 0.5 ns running averages of total bilayer surface tension vs time for systems with area/lipid of 0.605 nm^2 (solid black), 0.620 nm^2 (dashed black), 0.635 nm^2 (dotted–dashed black), 0.650 nm^2 (solid gray), and 0.665 nm^2 (dashed gray).

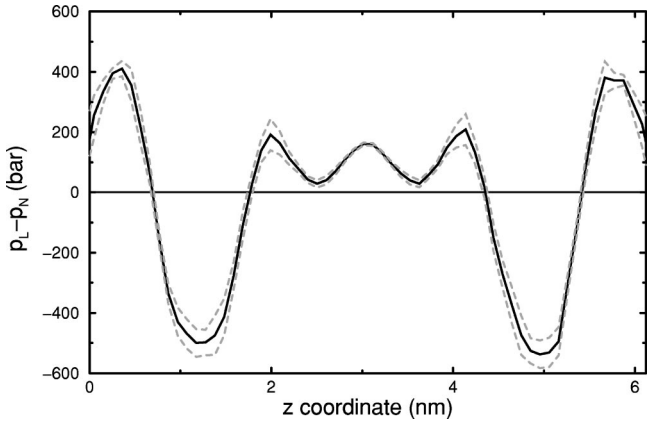

FIG. 5. Difference between lateral and normal pressure as a function of the normal coordinate in the membrane. The total pressure is drawn in solid black and the upper and lower standard deviation in dashed gray.

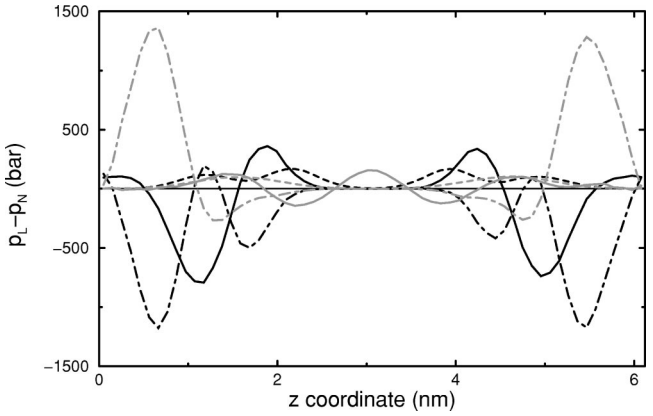

FIG. 6. Lateral pressure difference in the membrane decomposed into contributions from pairs of groups: Headgroup interactions (solid black), head–chain (dashed black), head–water (dotted–dashed black), chain (solid gray), chain–water(dashed gray), and water (dotted–dashed gray).

$$F(A) = F(A_0) + \frac{K_A}{2A_0}(A - A_0)^2. \tag{4.3}$$

Using the value of K_A above we see that the free energy will only increase by 0.05 kJ/mol lipid if the area per lipid is changed 0.02 nm^2 from its equilibrium value. For the 64–72 lipid systems common in many simulations this is just 1–1.25 k_BT, and they will thus exhibit substantial fluctuations in area. It is a very hard challenge for force fields to exactly reproduce the position of a minimum with a free energy curve this flat.

Figure 5 displays the total difference between lateral and normal pressure calculated from the local virial, $p_L(z) - p_N(z)$, which is directly related to the average surface tension through Eq. (2.1). The curve is obtained by a five point running average in space of the local pressure calculated in 60 z-slices for the system at 0.635 nm^2/lipid. The net surface tension in the order 10 mN/m corresponds to an average pressure difference of about 16 bar in the current systems; the spatial variations are 30 times larger. Comparing with the densities in Fig. 2 it is evident that the headgroups are contracting the system (negative lateral pressure, positive surface tension) while the chains expand it. There is also a positive lateral pressure in the headgroup–water interface, which does not entirely decrease to zero before reaching the box sides.

This suggests the bilayer is not completely hydrated, despite the water density reaching its bulk value. Zero surface tension in the middle of the water region would be attained by adding another 4–5 water molecules per lipid, increasing the water spacing to 3 nm. Some experiments on multilamellar systems[32] indicate lower values of roughly 2 nm, but the corresponding difference in total surface tension is small, only 1–2 mN/m (below our statistical accuracy), which could explain why the effective experimental equilibrium is reached already at lower hydration.

The lateral pressure difference is decomposed into the contributions from pairwise combinations of groups summed over interactions in Fig. 6 and for the different types of interactions summed over groups (electrostatics, 1–4 bonded interactions, Lennard-Jones, Ryckaert–Bellemans, other bonded forces, and SHAKE) in Fig. 7. The individual terms show variations which are an order of magnitude larger than their sum; local peaks exceed 4000 bars or 300 times the average pressure. By integrating the pressure differences according to Eq. (2.1) we obtain the total surface tensions listed in Table I. The energetic part of each tension term in the table was determined from linear regressions of partial energies versus area, exemplified for the chain Lennard-Jones interactions in Fig. 8. The standard errors in the energies are relatively small, although there are long time fluctuations which are hard to quantify accurately. However, since the surface tensions correspond to derivatives of free energy versus area the final accuracy determined from the standard error of the slope in the linear regression is considerably worse. The slope in Fig. 8 gives a surface tension of 139 ± 13 mN/m (an error of about 10%), but for many smaller contributions the relative uncertainty can be as large as 20%–50%. We have additionally solved for the remaining entropic part for each entry by using Eq. (2.8), although the group decomposition in this case is slightly artificial. It is

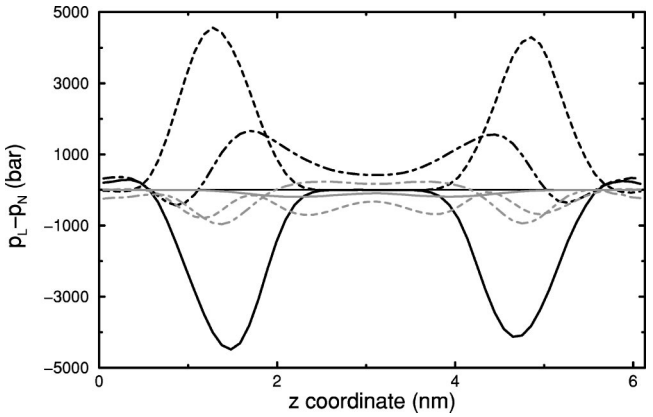

FIG. 7. Lateral pressure difference in the membrane decomposed into different types of interactions: Electrostatics (solid black), 1,4-interactions (dashed black), Lennard-Jones (dotted–dashed black), Ryckaert–Bellemans (solid gray), other bonded interactions (dashed gray), and SHAKE (dotted–dashed gray). The energy density anisotropy correction is included in the last term.

TABLE I. Calculated energetic and entropic terms of the bilayer surface tension in the 0.635 nm^2/lipid system. The energy density anisotropy has been added to the tail SHAKE term. The 1,4 interactions have not been separated into electrostatics and Lennard-Jones, since the latter contributes less than a percent.

Interaction		Surface tension (mN/m)		
Group	Type	Energetic	Entropic	Total
Chain	Lennard-Jones	139±13	−296±13	−157±2
	Angles	−5±4	155±4	150±3
	Ryckaert–Bellemans	57±10	−8.5±10	48.5±0.3
	SHAKE		−61±2	−61±2
Chain–head	Lennard-Jones	18±19	−122±19	−104±1
Chain–water	Lennard-Jones	−98±7	74±7	−24±1
Head	Angles and Dihedrals	−5±4	76±5	71±5
	SHAKE		184±6	184±6
	Lennard-Jones	220±4	−236±5	−16±2
	Electrostatics	592±171	92±171	684±8
	1,4-interactions	−102±27	−696±30	−798±14
Head–water	Lennard-Jones	−110±5	72±7	−38±5
	Electrostatics	−1257±188	1465±188	208±4
Water	SETTLE		−9±5	−9±5
	Lennard-Jones	42±5	−64±7	−22±4
	Electrostatics	680±79	−789±79	−109±2
Total		171±80	−163±80	8±5

nevertheless possible to use this data for a coarse separation of essentially independent entropic effects in the chain and headgroup/water regions. The entropic surface tension in the membrane totals to roughly −160 mN/m. Inserting this in Eq. (2.13) leads to a bilayer thermal expansivity of about 2×10^{-3} K^{-1}, which is within the relatively large range of experimental values[3] $1-6\times10^{-3}$ K^{-1}.

B. Headgroup and headgroup–water interactions

The energetic surface tension terms are huge in the outer part of the membrane where they are mainly due to electrostatics; intra-headgroup and intra-water interactions both give very large positive contributions to the tension, but they are opposed by an equally large negative term between headgroups and water. Another small negative term is obtained from half the Lennard-Jones interactions with the chain region. Interestingly, this seems to make the resulting sum almost negligible compared to the constituents, about 20 mN/m in the present case. The entropic terms are also of opposing signs, with large negative tensions from water and headgroups separately and a positive one between them. The resulting entropy is considerably smaller, but clearly positive. Depending on the amount of entropy from interactions with the chains included, we obtain a net result in the order 70–90 mN/m. Relating this to the curves in Figs. 6 and 7 we see that the intra-headgroup lateral pressure is contractive and located mainly at the position of the phosphocholine dipoles, but there is also a repulsive counterpressure located in the water region. This appearance is probably caused by the distribution of the entropy, where the water contribution is located further out than the headgroup and mixed terms. The remaining part is a small expanding contribution at the carbonyl dipoles, but this is largely cancelled by headgroup–water interactions. The total surface tension in the headgroup region is contractive and adds up to about 100 mN/m.

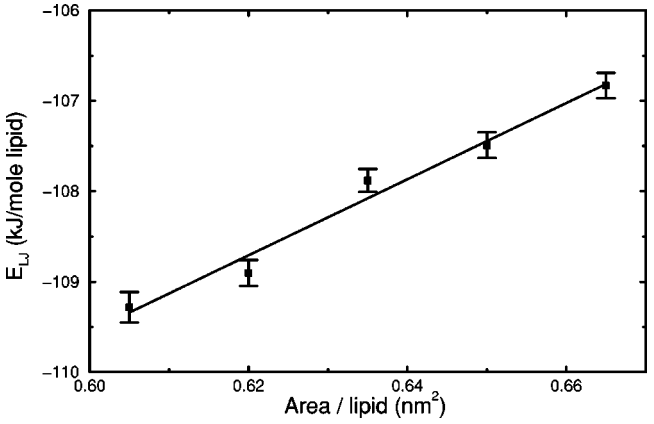

FIG. 8. Lennard-Jones energy between lipid chains plotted vs the area per lipid. The individual error bars are determined from the fluctuations and their autocorrelation times. A linear regression corresponding to Eq. (2.9) gives a slope 42±4 kJ/(mole lipid)/nm^2, where the confidence interval is determined from the standard error in the regression slope. Converted to standard units this is a surface tension of 139±13 mN/m (dyn/cm) for the entire bilayer. The other energetic contributions in Table I have been obtained similarly.

The physical background for these values is a combination of the solvation process and possibly headgroup dipole ordering. When the interfacial area is increased, water penetrating into the headgroups leads to a large gain of electrostatic energy from interactions between the polar headgroups and water. This is however compensated by a simultaneous loss of electrostatic interactions inside headgroups and water separately. A similar argument holds for the Lennard-Jones energies if the interactions with the chains are included. There is thus no significant change of solvation energy in the headgroup/water regions upon small changes in area close to the equilibrium state. The remaining positive energetic term (20–60 mN/m, depending on whether interactions with chains are included) might not be statistically significant, but it could represent changes in electrostatic interactions be-

TABLE II. Approximate main bilayer surface tension contributions in the headgroups (hydration and dipoles) and lipid chains. The dipole energy is not statistically significant, but a possible term from ordering in the headgroups.

Interaction	Surface tension (mN/m)
Hydration entropy	80
Dipole energy	20
Chain *gauche* energy	60
Other chain energy	90
Chain *gauche* entropy	−80
Other chain entropy	−160

tween the headgroup dipoles due to their ordering. This can be estimated through lattice sums on a two-dimensional hexagonal grid; an upper bound of about 120 mN/m has been suggested[6] since this value will be decreased for a more disordered lattice and screening of the dipoles from the polarized solvent molecules.

The major part of the entropy change upon water penetration is also a redistribution from water–water and headgroup–headgroup interactions to water–headgroup ones. The total entropy decreases with increasing area since water molecules at the interface become more ordered in the strong fields of the headgroup dipoles. There might also be an effect from water reorientation to regenerate the hydrogen bonds lost upon solvation of the hydrophobic core,[33,34] but this effect will be weaker than at a pure hydrocarbon–water interface considering the small overlap between water and chain density in Fig. 2. In a bilayer the main interactions will instead be with the headgroups which work as an efficient barrier preventing waters from entering the membrane interior. Despite the slightly different process, semiempirical models from pure hydrocarbon solubility data[6] suggest values of 70–100 mN/m which agree well with our calculated overall hydrational surface tension.

These estimated main contributions to surface tension in the different bilayer regions are summarized in Table II. The most important one in the headgroups is the contraction, which reasonably should be a general feature of lipid systems. The opposing entropic term in the water region might however also be important, since it will help stabilizing the bilayer due to the resulting positive–negative–positive lateral pressure profile on each side. This can be compared with simplified bilayer models[35,36] in which the system consists of pointlike solvent particles and surfactants with a few interactions sites. Such setups successfully reproduce the main contracting effect in the headgroup/water interface, but not the separation of entropy causing the partial positive lateral pressure in the solvent since this is probably dependent on the exact hydrogen-bond geometry of water molecules.

C. Chain and chain–headgroup interactions

The energetic surface tension in the bilayer interior consists of contractive contributions from Lennard-Jones interactions and Ryckaert–Bellemans dihedrals. Adding bonded forces and half the interactions with headgroups gives a total energetic surface tension about 150 mN/m in our simulations. This is opposed by larger expansion terms due to

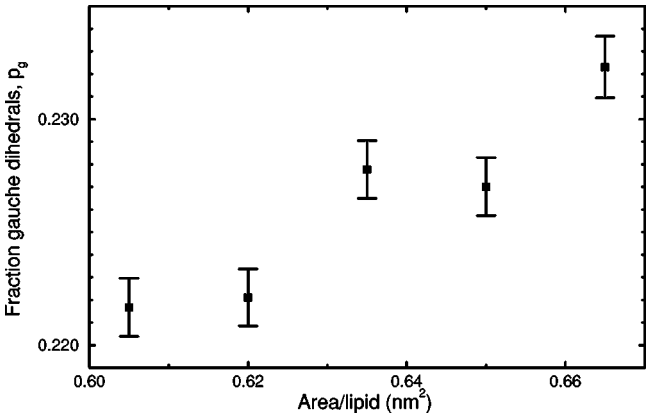

FIG. 9. Average fraction of dihedrals in the *gauche* state in the lipid chains displayed vs area/lipid. The error bars have been calculated from the standard deviations corrected for the autocorrelation time. The solid line is the linear regression vs area.

gauche and chain conformational entropy, making the total surface tension in the chain region negative, in the order of −100 mN/m (roughly the same as the contraction in the interface region, but with opposite sign). The spatial distribution shows that the corresponding lateral pressure has peaks both in the center of the membrane and a bit up in the chains. Since the chains are attached to the lower part of the headgroups their decomposition is somewhat artificial, and the innermost charged carbon atoms which contribute an expansive lateral pressure might possibly be better characterized as belonging to the chain region.

The Ryckaert–Bellemans contribution is directly related to the area dependence of *gauche* bond fraction in the chains. This could in principle be verified by measuring the *gauche* bond contents through Raman on IR spectroscopy, but it is not easy to interpret the experimental results and arrive at a reliable figure. There is further a large spread in both experimental and simulated values. Our five systems exhibit values of 22.17%, 22.21%, 22.78%, 22.70%, and 23.23% in order of increasing area. This is displayed vs the area per lipid in Fig. 9; note the clear correlation with the surface tension in Fig. 4 due to long time correlations. The *gauche* fraction in many other simulations lies in the range 15%–25% while experimental IR data[37–39] on the contrary indicate average gauche fractions of 28%–33%, but with large uncertainties. An alternative way of estimating the *gauche* contents is to use the phase transition entropy, which is easily obtained from the enthalpy and temperature of the phase transition. We assume (i) there are no other contributions than *trans-gauche* isomerizations to the entropy change, and (ii) the entropy can be calculated from a simple model where there are no correlations between bonds at different positions in a chain or between different chains. Then the entropy per lipid as a function of the fraction *gauche* bonds, p_g, will be[40]

$$\Delta S = N_b k_B (p_g \ln 2 - p_g \ln p_g - (1-p_g)\ln(1-p_g)). \tag{4.4}$$

N_b is the number of dihedral bonds in the two chains of a lipid, $2 \cdot 13 = 26$. The experimental value of the phase transition enthalpy[41] is about $\Delta H = T_m \Delta S = 36$ kJ/mol, which corresponds to an entropy change of 13.7 k_B. The *gauche* bond

contents in the gel phase is uncertain; Eq. (4.4) yields 15% *gauche* bonds in the liquid phase if we neglect it, or 25% if we use data from vibrational Raman spectroscopy indicating two *gauche* bonds per gel phase DPPC lipid.[42] Since the assumptions in the preceding paragraph are questionable (and any correlations will decrease entropy, leading to a higher *gauche* fraction) the results should be considered an estimate. Nevertheless the interval 15%–25% is in agreement with the present simulations and supports a smaller value than reported from spectroscopic models.

The corresponding entropic surface tension term can be calculated from the area dependence of Eq. (4.4). Using the simulated *gauche* bond fractions at the five different areas results in a bilayer tension of approximately -80 mN/m. As for the average *gauche* contents above this is a lower bound, and other entropic contributions could justify a higher magnitude. However, this term can additionally be estimated from mean-field theories[43,44] with rotational isomeric states and uniform segment density. For 16 carbon atoms and an area of 0.3 nm^2 per chain, this also gives roughly -80 mN/m, which indicates the other entropic contributions should be relatively small. The mean-field model also reproduces the two positive peaks in the upper part of the lipid tails due to the distribution of segments around which there are dihedral potentials. (The peak in the center is in contrast explained by the reduction of the bond angle contribution due to the lower density.)

While the *trans–gauche* transitions determine the main dynamics inside each chain the nonbonded interactions dominate the interchain pressure, and to explain this dynamics we need a model for their energy. Nagle has suggested a description of the change in the Lennard-Jones energy during the phase transition based upon the approximate 5% increase in volume (about 1/6th of simultaneous relative area change).[45] Assuming linearity this would lead to a surface tension about 100 mN/m, but a major part of the volume change is probably occurring closer to the gel phase area. In the present simulations the relative volume change around the equilibrium area is much smaller, less than a third of the above value, corresponding to a smaller surface tension. In Appendix B we show how a simplified but explicit model of the Lennard-Jones interactions between neighboring chains can give rise to a contracting contribution up to 200 mN/m even at constant volume, due to the differences in pair correlation functions in directions parallel and normal to the bilayer. This approach overestimates the tension, so the true process is probably a combination of the two models with the constant volume/parallel chains view being more appropriate in the upper part of the chains and the Lennard-Jones gas a better description in the bilayer center. It is however reassuring that they yield similar energies and surface tensions in the same order of magnitude.

The conformational entropy between chains is much harder to estimate theoretically since it is very dependent on their exact geometry, but the dominating contribution should be due to steric interactions of the carbon atoms. The entropic pressure from such steric repulsions has been estimated to another -80 mN/m by using semiempirical models from molecular dynamics of hard disks.[46] This still leaves an entropic term in the order of -80 mN/m from chain interactions which is unaccounted for, compared with the present simulations. From Fig. 6 it is evident that a large part of the chain pressure is located as far out as the carbonyl dipoles, suggesting this could be a contribution from headgroup orientational entropy. It is however also possible that the model above underestimates the steric repulsive pressure or the bilayer could experience collective entropic effects from *gauche* bonds despite the earlier conclusions. The total surface tension in the chain region is thus in the order of -90 mN/m if we include half the interactions with headgroups, almost canceling the interfacial contraction. We expect this overall expansion to be a common behavior in lipid chains, unless the headgroups are very large compared to the chains, in which case the lipids will prefer to form micelles. On a more detailed level, it is at least plausible that the several pressure peaks in the bilayer interior is a common feature, since they are reproduced not only in simplified model systems,[35,36] but even by mean-field theories.[44]

D. Relation to the bilayer phase transition

Our simulation results and the Lennard-Jones model make some interesting comparisons with experimental data on the main lipid bilayer phase transition possible. The experimental enthalpy change at the transition of DPPC from gel to liquid crystalline phase is about 36 kJ/mol, while the area changes from 0.47 to 0.63 nm^2 per lipid.[41] Taking the area dependence of the nonbonded chain energy from our model in Appendix B gives $\Delta H_{LJ} \approx 20$ kJ/mol. Using the Lennard-Jones gas model[45] produces almost the same value, 23 kJ/mol. To this we may add the contribution from chain-headgroup/water interactions and possibly the headgroup dipolar term. This will slightly lower the value, say 15–20 kJ/mol considering the large uncertainty of the area dependence in these terms. The other contribution comes mainly from the increase in chain bond *gauche* conformations by 15–25 units of percent, yielding 13–19 kJ/mol depending on the *gauche* contents in the gel phase. These results indicate a lower fraction *gauche* bonds than calculated from experimental models. Essentially all the measured enthalpy of the phase transition is thus accounted for by the chain Lennard-Jones and *gauche* energies. This is reasonable since these are the only terms approximately proportional to chain length ($N-1.7$ and $N-3$, respectively). The experimental phase transition enthalpy goes as $N-7$, but this is influenced by the dependence of transition temperature on chain length; alternatively the difference could be ascribed to negative terms independent of chain length, possibly the interactions with headgroups and water. Regardless of the origin of this correction, the present simulations are in agreement with the view that the phase transition is predominantly a process in the hydrophobic core, without much influence from the headgroups or solvent.[47] This is also supported by the estimated area dependence of main contributions to surface tension like those in Table II; Marsh suggests[6] that all magnitudes decrease with larger area, except for the hydration term which should be essentially constant.

V. CONCLUSIONS

The calculation of a space-dependent virial makes it possible to determine local pressures and surface tension uniquely at least down to scales of about a nanometer in molecular dynamics simulations. The resulting surface tension is a combination of energetic and entropic terms, where the energetic parts can be determined independently from the area dependence of groupwise interaction energies by performing simulations at several different areas.

We have used this to explore the interactions and decompose the surface tension groupwise and spatially in a hydrated 256 lipid dipalmitoylphosphatidylcholine bilayer.

The resulting net bilayer surface tension in the simulations is a delicate balance between contracting forces in the headgroup/water region and an expansion in the lipid chains. The lateral pressure in the interfacial part of the bilayer is almost entirely explained by entropic solvation effects caused by electrostatic interactions. This yields a total surface tension in the order of 100 mN/m from the outer part of the membrane. The main contracting part of this is located at the position of the headgroups, but there is also an important expansive region in the solvent immediately outside the lipids. The latter is an interesting observation from the simulations, since it might help to stabilize the bilayer due to the resulting positive–negative–positive lateral pressure profile if it is present also in real bilayer systems.

In the lipid chains we find that the Lennard-Jones and dihedral energies are contracting the bilayer (contributing about 150 mN/m in the DPPC simulations), but this is outweighted by large entropic terms making the total surface tension in the hydrophobic core expansive, roughly -90 mN/m. The interactions between chains and solvent are found to be much smaller than at a pure hydrocarbon interface since the headgroups work as an efficient barrier preventing water from penetrating the DPPC membrane interior.

Resolving the local pressure shows that the spatial variations of the surface tension constituents are huge, several orders of magnitude above the resulting average. Although the overall surface tension in a particular simulation can be calculated to an error of a few mN/m, this means the inherent accuracy of the force field used could be much worse. This is especially severe for lipid bilayers, since the contracting force in the interfacial region comes almost entirely from electrostatic interactions while the expansion in the interior only depends on the Lennard-Jones and *trans–gauche* energy difference. Even with good models for these interactions, any discrepancy between the two types of interactions will be at least tenfold magnified in the final balance, explaining the sensitivity of simulation surface tension to details in setup.

This balance between predominantly entropic pressures should be one of the main physical characteristics of lipid assemblies. It also suggests why simplified model systems are reasonably good at reproducing the general shape of the pressure curves, since the signs of the entropic contributions mainly depend on the relative size and orientation of different parts of the surfactants. Our simulations also indicate that the phase transition properties of the DPPC bilayer studied can be deduced almost entirely from the chain region dynamics, without much influence from the headgroups or solvent. The headgroup geometry in a specific lipid should instead be important to determine whether the equilibrium conformations are micelles, bilayers or hexagonal phases, depending on the relative size of local pressures in the contracting and expanding regions. These properties should be possible to test in future computer simulations by resolving the lateral pressure for different types of lipids and other force fields.

ACKNOWLEDGMENTS

We are grateful to John Nagle for several worthwhile discussions. This work was supported with computing resources by the Swedish Council for Planning and Coordination of Research (FRN) and Parallelldatorcentrum (PDC), Royal Institute of Technology.

APPENDIX A: LOCAL PRESSURE IN THE SIMULATIONS

The macroscopic pressure tensor in a system can be written as

$$\mathbf{p}=\frac{1}{V}\sum_i m_i\mathbf{v}_i\otimes\mathbf{v}_i-\mathbf{\Sigma}, \tag{A1}$$

where the first term is a sum over particles and the second the ensemble average of the interactional stress tensor of the system, which in the case of pairwise forces evaluates to $\langle\sigma\rangle=1/V\Sigma_{i<j}\mathbf{F}_{ij}\otimes\mathbf{r}_{ij}$. It is straightforward to extend this definition to local pressure on scales longer than the significant range of molecular interactions. Below this, we need an explicit definition of the microscopic stress tensor σ. Schofield and Henderson[48] have derived a local expression with an attractive similarity to the macroscopic stress,

$$\sigma(\mathbf{r})=-\sum_i \mathbf{F}_i\otimes\int_{\mathcal{C}_{0i}}\delta(\mathbf{r}'-\mathbf{I})dl, \tag{A2}$$

where the integral is taken over contours $\mathcal{C}_{0i}$ from an arbitrary $\mathbf{r}_0'$ to the position $\mathbf{r}_i$ of each particle. We choose one of the particles for the reference position and then average this over all particles to get

$$\sigma(\mathbf{r})=-\frac{1}{2}\sum_{i\neq j}\mathbf{F}_{ij}\int_{\mathcal{C}_{ij}}\delta(\mathbf{r}'-\mathbf{I})dl. \tag{A3}$$

It is relatively easy to derive similar expressions for interactions of any finite order,[35] but not long range lattice sums. The ordinary Coulomb interaction is pair-additive, but when the charges are transformed and the potential solved in reciprocal space the individual contributions will not be simple sums over low-order interactions but rather the number of atoms in the whole system. Although theoretically possible it is not a practical alternative to calculate interactions of such an order. Further, the reciprocal-space virial contributions do not have uniquely defined spatial locations. Although it is probably possible to circumvent these shortcomings by modifying the algorithm it is far from trivial and this presently excludes lattice summations when calculating local pressures. In the present simulations we have instead chosen to use long cutoffs, in which case it is easy to decompose all

forces into pairwise interactions with well defined spatial locations. For usual force fields it is not necessary to deduce the higher-order expressions even for bond angles or dihedrals, since these can also be rewritten as sums of pairwise interactions. The virial contribution from the bond constraining algorithm was extracted by calculating the forces corresponding to the coordinate changes applied in each iteration of the algorithm, $\Delta \mathbf{F}_i = m_i \Delta \mathbf{r}/(\Delta t)^2$.

Since the membrane is homogeneous and isotropic in the lateral (x,y) plane we only need to resolve the microscopic stress as a function of the normal, z, coordinate. By dividing the box into slices of thickness Δz along the normal and choosing linear contours parametrized as $l = \mathbf{r}_i + \lambda \mathbf{r}_{ij}$, the stress tensor evaluates to[35]

$$\sigma(z) = \frac{1}{\Delta V} \sum_{i<j} \mathbf{F}_{ij} \otimes \mathbf{r}_{ij} f(z, z_i, z_j), \tag{A4}$$

where ΔV is the volume of each slice. $f(z,z_i,z_j) = \Delta z/|z_i - z_j|$ if both particles are outside the current slice on opposite sides (imposing periodic boundary conditions), $f(z,z_i,z_j) = \Delta z/2|z_i - z_j|$ if one of them is in the slice and $f(z,z_i,z_j) = 1$ if both positions are inside the slice. Finally, when both particles are outside the slice on the same side there is no contribution to the local virial. A local virial tensor corresponding to Eq. (A4) was implemented in the molecular dynamics software and separated into contributions from forces due to different interaction types and groups of atoms. In the simulation the contributions are most practically assigned the other way around, though; for each pairwise force calculated the virial is determined and then distributed in slices between the two interaction positions according to Eq. A4.

APPENDIX B: ENERGETIC CONTRIBUTIONS TO SURFACE TENSION FROM LENNARD-JONES INTERACTIONS

The energetic contribution to surface tension from nonbonded interactions in the lipid chains can be estimated through a simplified model in which each chain is replaced by a rigid rod with N beads at distance a. These rods are tilted an angle θ and placed parallel on a hexagonal lattice. The average distance d between two rods in the direction perpendicular to the rod vector can be calculated from the area per lipid (two chains) through the relation

$$A \cos\theta = \sqrt{3} d^2. \tag{B1}$$

If we assume the volume per CH_2 group to be constant, a can be expressed in terms of the area as

$$a = \frac{2 V_{CH_2}}{A \cos\theta}. \tag{B2}$$

The van der Waals energy between two interacting rods at distance d is then summed up, multiplied by the number of nearest neighbors (6) and divided in half to obtain the energy per chain

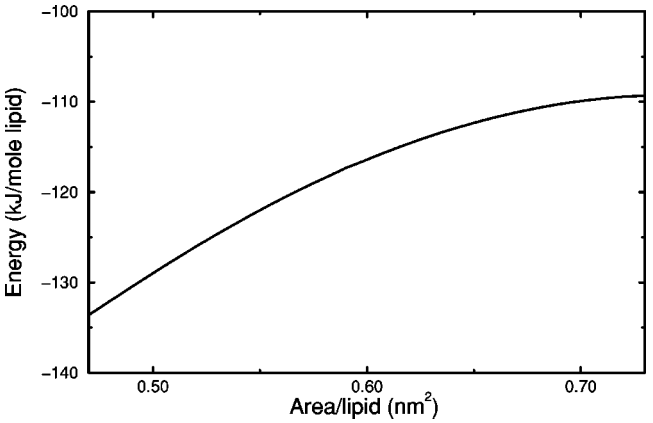

FIG. 10. Area dependence of the Lennard-Jones energy from the chain interaction model in Appendix B.

$$U_{\mathrm{vdW}} = -12\epsilon\sigma^6 \sum_{i,j=1}^{N} \frac{1}{|\mathbf{r}_i - \mathbf{r}_j|^6} = -12\epsilon\sigma^6 \sum_{i,j=1}^{N} \frac{1}{[(i-j)^2 a^2 + d^2]^3}, \tag{B3}$$

where ϵ and σ are the usual Lennard-Jones parameters. This sum can be converted to a single sum over the index $k = i - j$, and then replaced with an integral approximation

$$U_{\mathrm{vdW}} = -12\epsilon\sigma^6 \sum_{k=-N}^{N} \frac{N - |k|}{[(ak)^2 + d^2]^3} = -12\epsilon\sigma^6 \int_{-N}^{N} \frac{N - |k|}{[(ak)^2 + d^2]^3} dk. \tag{B4}$$

Putting the integration interval to $[-\infty, \infty]$ introduces an error less than 1% when $N = 16$ and yields

$$U_{\mathrm{vdW}} = -\frac{3\epsilon\sigma^6 (3Na\pi - 4d)}{2a^2 d^5}. \tag{B5}$$

The corresponding expression for the repulsive r^{-12} interactions can be calculated analogous to

$$U_{\mathrm{rep}} = \frac{3\epsilon\sigma^{12} (315Na\pi - 256d)}{320a^2 d^{11}}. \tag{B6}$$

Both parameters a and d can be expressed in terms of the surface area through Eqs. (B1) and (B2). The chain tilt angle θ is 32° in the gel phase[49] at 0.47 nm^2/lipid. In the high-temperature phase the chains are more disordered, randomly rotated, and nontrivial to model. As a rough approximation we use the average order parameters in the chains to calculate an effective angle slightly above 40°. The exact dependence on area is not known, but we assume a linear variation of $\cos^2\theta$ as in models of order parameters.[11,50] Using $N = 16$, $V_{CH_2} = 0.0276$, $\sigma = 0.396$ nm, and $\epsilon = 0.38$ kJ/mol from the force field we have plotted the total chain Lennard-Jones energy $U_{\mathrm{LJ}} = U_{\mathrm{vdW}} + U_{\mathrm{rep}}$ as a function of area in Fig. 10. At the equilibrium area in the liquid phase we get

−113 kJ/mol lipid, in fair agreement with the simulation result −108 kJ/mol lipid. The attracting energy will approximately be proportional to $N-1.7$ and the repulsive to $N-1$.

It is also straightforward to calculate the surface tension by taking the derivative of total energy with respect to A (note the A dependence in the parameters a and d). For a bilayer this yields $\gamma_{LJ}\approx 230$ mN/m at $A=0.63$ nm^2. This is clearly too large compared to the simulations, but still in the right order of magnitude. The surface tension in the model is about 500 mN/m at the area corresponding to the gel phase, and then decreasing with larger area. The simulation value 140 mN/m is reached first at 0.68 mN/m. This is not surprising, though, since the derivative of the energy is more sensitive to the exact area dependence of the chain tilt angle than the energy itself. Further, the approximation of completely parallel chains in the liquid crystalline phase is questionable especially in their lower part, but the result is nevertheless useful as a first-order model.

One could ask if the Lennard-Jones interactions along/inside each chain would work in the opposite way and lower the net surface tension. However, since the closest three neighbors in each direction are excluded the resulting magnitude will be small, in the order 10–20 mN/m. This is less than the inherent errors in the model and we have thus chosen to neglect it.

The Lennard-Jones interactions of the chains with head groups and external water can be represented in a continuum picture. A straightforward calculation with a few minor approximations gives the contribution

$$\gamma_{surr}=-\frac{4\pi\epsilon\sigma^4\rho}{3V_{CH_2}}\approx -80 \text{ mN/m}, \tag{B7}$$

where ρ is the number density in the surrounding medium. Since this is largely compensated for by opposite changes inside each group we assign half to the chain region and half to headgroup/water.

The conclusion from this is that it is possible to obtain a surface tension from chain Lennard-Jones interactions, even when the volume per lipid is approximately constant. The main physical basis for this is the pair correlation function of interacting hydrocarbons being different in directions perpendicular and parallel to the membrane normal. Energetically, this simplified model gives a total positive surface tension in the order 150–200 mN/m from Lennard-Jones interactions in hydrocarbon chains and with their surroundings, depending on how much of the headgroup/water term we include.

[1] R. B. Gennis, *Biomembranes: Molecular Structure and Function, Springer Advanced Texts in Chemistry* (Springer, New York, 1989).
[2] S. A. Safran, *Statistical Thermodynamics of Surfaces, Interfaces, and Membranes, Frontiers in Physics* (Addison–Wesley, Reading, 1994).
[3] M. Bloom, E. Evans, and O. G. Mouritsen, Q. Rev. Biophys. **24**, 293 (1991).
[4] E. Evans, Langmuir **7**, 1900 (1991).
[5] E. Lindahl and O. Edholm, Biophys J. **79**, 426 (2000).
[6] D. Marsh, Biochim. Biophys. Acta **1286**, 183 (1996).
[7] T. R. Stouch, K. B. Ward, A. Altiera, and A. T. Hagler, J. Comput. Chem. **12**, 1033 (1991).
[8] T. R. Stouch, Mol. Simul. **10**, 335 (1993).
[9] K. Tu, D. J. Tobias, J. K. Blasie, and M. L. Klein, Biophys. J. **70**, 595 (1996).
[10] D. P. Tieleman, S. J. Marrink, and H. J. C. Berendsen, Biochim. Biophys. Acta **1331**, 235 (1997).
[11] O. Berger, O. Edholm, and F. Jähnig, Biophys. J. **72**, 2002 (1997).
[12] S. E. Feller and R. W. Pastor, J. Chem. Phys. **111**, 1281 (1999).
[13] S. E. Feller and R. W. Pastor, Biophys. J. **71**, 1350 (1996).
[14] F. Jähnig, Biophys. J. **71**, 1348 (1996).
[15] J. G. Kirkwood and F. P. Buff, J. Chem. Phys. **17**, 338 (1949).
[16] S. Nosé and M. L. Klein, Mol. Phys. **50**, 1055 (1983).
[17] W. van Gunsteren and M. Karplus, Macromolecules **15**, 1528 (1982).
[18] W. van Gunsteren and H. J. C. Berendsen, *Groningen Molecular Simulation (GROMOS) Library Manual* (Biomos, Groningen, 1987).
[19] S. Chiu, M. Clark, V. Balaji, S. Subramaniam, H. Scott, and E. Jakobsson, Biophys. J. **69**, 1230 (1995).
[20] J. Ryckaert and A. Bellemans, Chem. Phys. Lett. **30**, 123 (1975).
[21] W. Jorgensen and J. Tirado-Rives, J. Am. Chem. Soc. **110**, 1657 (1988).
[22] H. J. C. Berendsen, J. P. M. Postma, A. DiNola, and J. R. Haak, J. Comput. Phys. **81**, 3684 (1984).
[23] H. J. C. Berendsen, D. van der Spoel, and R. van Drunen, Comput. Phys. Commun. **91**, 43 (1995).
[24] B. Hess, H. Bekker, H. J. C. Berendsen, and J. G. E. M. Fraaije, J. Comput. Chem. **18**, 1463 (1997).
[25] S. Miyamoto and P. A. Kollman, J. Comput. Phys. **13**, 952 (1992).
[26] J. P. Ryckaert, G. Ciccotti, and H. J. C. Berendsen, J. Comput. Phys. **23**, 327 (1977).
[27] R. Goetz, G. Gompper, and R. Lipowsky, Phys. Rev. Lett. **82**, 221 (1999).
[28] R. Lipowsky and S. Grotehans, Biophys. Chem. **49**, 27 (1994).
[29] J. N. Israelachveli and H. Wennerström, J. Phys. Chem. **96**, 520 (1992).
[30] E. Evans and W. Rawicz, Phys. Rev. Lett. **64**, 2094 (1990).
[31] W. Rawicz, K. Olbrich, T. McIntosh, D. Needham, and E. Evans, Biophys. J. **79**, 328 (2000).
[32] H. I. Petrache, N. Gouliaev, S. Tristram-Nagle, R. Zhang, and R. M. Suter, Biophys. J. **57**, 7014 (1998).
[33] H. S. Frank and M. W. Evans, J. Chem. Phys. **13**, 507 (1945).
[34] C. Tanford, *The Hydrophobic Effect* (Wiley, New York, 1980).
[35] R. Goetz and R. Lipowsky, J. Chem. Phys. **108**, 7397 (1998).
[36] M. Venturoli and B. Smit, PhysChemComm. **2**, www.rsc.org/ej/qu/1999/I9906472/index.htm (1999).
[37] R. Mendelsohn, M. A. Davies, J. W. Brauner, H. F. Schuster, and R. A. Dluhy, Biochemistry **28**, 8934 (1989).
[38] R. Mendelsohn, M. A. Davies, H. F. Schuster, Z. Xu, and R. Bittman, Biochemistry **30**, 8558 (1991).
[39] H. L. Casal and R. N. McElhaney, Biochemistry **29**, 5423 (1990).
[40] P. J. Flory, *Statistical Mechanics of Chain Molecules* (Wiley, New York, 1969).
[41] R. Ladbrooke, R. Williams, and D. Chapman, Biochim. Biophys. Acta **150**, 333 (1968).
[42] N. Yellin and I. W. Levin, Biochemistry **16**, 642 (1977).
[43] D. R. Fattal and A. Ben-Shaul, Biophys. J. **65**, 1795 (1993).
[44] I. Szleifer, D. Kramer, and A. Ben-Shaul, J. Chem. Phys. **92**, 6800 (1990).
[45] J. F. Nagle, J. Chem. Phys. **58**, 252 (1973).
[46] W. G. Hoover and F. H. Ree, J. Chem. Phys. **49**, 3609 (1968).
[47] J. F. Nagle, Annu. Rev. Phys. Chem. **31**, 157 (1980).
[48] O. Schofield and J. R. Henderson, Proc. R. Soc. London, Ser. A **379**, 231 (1982).
[49] S. Tristram-Nagle, R. Zhang, R. M. Suter, C. R. Worthington, W.-J. Sun, and J. F. Nagle, Biophys. J. **64**, 1097 (1993).
[50] J. F. Nagle, Biophys. J. **64**, 1476 (1993).